

# ENERGY STORAGE AND HARVESTING IN SrTiO<sub>3</sub>/ EPOXY NANODIELECTRICS

G. C. Manika, G. C. Psarras

Smart Materials & Nanodielectrics Laboratory, Department of Materials Science,  
University of Patras, 26504, Patras, Greece  
Email: [manikage@upatras.gr](mailto:manikage@upatras.gr), [G.C.Psarras@upatras.gr](mailto:G.C.Psarras@upatras.gr)

**Keywords:** SrTiO<sub>3</sub> nanoparticles, dielectric response, energy harvesting

## Abstract

Composite nanodielectric materials with strontium titanate nanoparticles embedded within an epoxy resin matrix were prepared and studied, varying the filler content. Broadband dielectric spectroscopy was employed for determining the dielectric response of the prepared specimens. Dielectric results reveal the presence of three relaxations processes, which are attributed to (a) glass to rubber transition of the polymer matrix ( $\alpha$ -mode), (b) re-arrangement of polar side groups ( $\beta$ -mode) and (c) interfacial polarization between systems' constituents. The stored and harvested energy of the examined nanodielectrics was also evaluated under DC conditions, in the applied voltage range of 10-240V. The coefficient of energy efficiency ( $n_{eff}$ ) was determined for all filler contents, varying the applied temperature and field. The effect of temperature appears to be pronounced causing a sigmoidal dependence of  $n_{eff}$ . Finally, filler content enhances  $n_{eff}$  reaching the highest value of 69.41% for the 10phr SrTiO<sub>3</sub> nanocomposite at 50V.

## 1. Introduction

Energy is one of the most important issues in the 21<sup>st</sup> century. The exhaustion of fossil fuels in combination with the increasing energy requirements leads to the necessity for immediate improvement at the energy efficiency. Nowadays, most of the produced energy is lost in terms of heat, mainly in electric power generation and transmission. Therefore, the improvement in the efficiency of energy usage plays a key role in energy systems [1-4]. Multifunctional polymer composites could be used as structural energy devices, where matrix and filler work synergistically for a better functional behavior. Nanostructured materials are becoming increasingly important for electrochemical energy storage and more specific in the electrochemical capacitors. Furthermore, nanostructured materials have attracted a lot of interest in recent years, because of their unusual mechanical, electrical and optical properties endowed by confining the dimensions of such materials and due to the combination of bulk and surface properties to the overall behavior. Dielectric nanocomposites derive their high energy density from the use of high dielectric constant filler and high breakdown strength polymer which, when combined in the correct ratio and dispersion, can achieve higher energy density than either of the constituents alone. Nanodielectrics refers to dielectric materials which comprise entities with dimension at the nanometric scale. The type and the amount of the nanoinclusions determine the dielectric behavior and for this reason polymer matrix nanocomposites attend enlarged technological and scientific interest, replacing conventional materials in a variety of applications [5-8].

Energy harvesting refers to “self-powered” devices requiring no external power for operation either continuous or punctuated, and no replaceable power supplies. Current portable and wireless devices must be designed in a specific way in order to include electrochemical batteries. Nanostructured

materials are very promising in the design of new innovative structures. Nanostructured materials impart improved capabilities to energy harvesting devices and it is expected that in the near future they will be a major driver in optimizing the energy efficiency [9]. The choice of an epoxy resin as a polymer matrix presents many advantages, such as the good thermomechanical behavior, the resistance to corrosive environments, low cost etc. Moreover, ceramic strontium titanate ( $\text{SrTiO}_3$ ) nanoparticles were chosen as the reinforced phase.  $\text{SrTiO}_3$  is a complex oxide having a perovskite structure. It has attracted a lot of interest because of its potential use in electronic devices, because of its high charge storage capacity, good insulating properties and good optical transparency in the visible region. In past years,  $\text{SrTiO}_3$  was widely used as a substrate for epitaxial growth of high temperature superconducting films.  $\text{SrTiO}_3$  is applicable in electronic devices not only as a high dielectric constant insulator, but also as a wide-gap semiconductor with a band gap of 3.2eV.  $\text{SrTiO}_3$  is a ferroelectric material in which its ferroelectric transition is suppressed by quantum fluctuation. At a critical temperature ( $T_c=104\text{K}$ ),  $\text{SrTiO}_3$  undergoes a cubic to tetragonal antiferrodistortive transition. The phase transition derives from the rotation of the oxygen octahedral around one of the cubic main axes, while two adjacent small cells are opposite [10,11].

In this work nanocomposites constituted of an epoxy resin (ER) as a matrix and strontium titanate ( $\text{SrTiO}_3$ ) nanoparticles as the reinforcing phase, have been prepared and studied at various filler contents.  $\text{SrTiO}_3$  nanoparticles were first studied via X-ray diffraction (XRD), differential scanning calorimetry (DSC) and laser Raman spectroscopy (LRS) and their dielectric response was examined via broadband dielectric spectroscopy (BDS). Furthermore, nanocomposite systems were studied by means of the same experimental techniques. The main goal of this work is to investigate the energy efficiency by determining the stored and harvested energy in nanocomposites with parameters the applied DC field, temperature and filler content.

## 2. Experimental

### 2.1 Fabrication of nanocomposite materials

Nanocomposite specimens were prepared by employing commercially available materials. A low viscosity epoxy resin with the trade name Epoxol 2004A, and a slow reacting cycloaliphatic amine as curing agent, with the trade name Epoxol 2004B, were used for the preparation of the polymer matrix. Both reactants were provided by the Neotex S.A. Athens, Greece. Nanoparticles of strontium titanate ( $\text{SrTiO}_3$ ) were purchased by Sigma Aldrich (nanoparticle diameter < 100nm). The followed procedure includes mixing the resin with the curing agent in a 2:1 (w/w) ratio. As the polymer matrix is in liquid state, various amounts of ceramic filler were added for the production of the nanocomposite specimens. Stirring at a slow stirring rate under ultrasonication was performed in order to avoid the formation of clusters. The homogenized mixtures were poured to moulds and the curing process took place at ambient conditions for a week, followed by post-curing at 100°C for 4h. The  $\text{SrTiO}_3$  content of the prepared samples was in parts per hundred resin (phr) per weight and the manufactured samples were: 0 (unreinforced epoxy), 1, 3, 7, 10, 12 and 15phr.

### 2.2 Methods

#### 2.2.1 Methods for structural analysis

XRD experiments were performed with a Bruker AXS D8 Advance device with Bragg-Bretano geometry. A LynxEye detector and Cu Ka spectral line ( $\lambda = 1.54062\text{\AA}$ ) was used as the incident radiation. Scan mode was continuous, the step was  $0.02^\circ$  2-theta and the scan speed was 0.5s/step. Source slit was 0.6mm while voltage and current were set at 40kV and 40mA respectively. The morphology and the quality of the nanoparticles dispersion, as well as the existence of agglomerates and voids inside the polymer matrix, were investigated by means of SEM (Carl Zeiss EVO MA 10). DSC measurements were conducted via a TA Q200 device (TA Instruments, New Castle, USA). The scan rate was 30°C/min

and the samples were placed in an aluminum crucible, while an empty one was used as reference. Temperature was ranging from  $-40^{\circ}\text{C}$  to  $200^{\circ}\text{C}$ . Raman experiments were held on a HR-800 JY UV-Vis-Raman system (Horiba Scientific, Jobin Yvon, Villeneuve d'Ascq, France), where excitation was imposed by an air cooled He-Cd laser operating at 441.6nm. The power of the laser beam was 0.23mW. The backscattered configuration was selected using a 50x (NA=0.55) microscope objective. The scattered beam was directed to the entrance slit of the single monochromators after passing through an appropriate edge filter. The signal was recorded by an LN2-cooled 2D-CCD detector.

## 2.2.2 Dielectric measurements

Broadband dielectric spectroscopy (BDS) was employed for the electrical characterization of all manufactured nanocomposites. The frequency range varied from 0.1Hz to 10MHz and an Alpha-N Frequency Response Analyzer was used, supplied by Novocontrol Technologies. The applied  $V_{\text{rms}}$  was constant at 1V, while the temperature was controlled by Novotherm system (Novocontrol Technologies) with  $\pm 0.1^{\circ}\text{C}$  accuracy. A two electrodes dielectric cell (BDS 1200), also supplied by Novocontrol, was used. The specimens were placed between the gold-plated metal electrodes and isothermal frequency scans were conducted for every specimen, from ambient to  $160^{\circ}\text{C}$  with a temperature step of  $5^{\circ}\text{C}/\text{min}$ . Data acquisition was performed automatically in real time via windeta software. All AC measurements were performed according to the ASTM D150 specifications.

DC measurements were conducted by a High-Resistance Meter, DC (Agilent 4339B). The experimental procedure includes an automatic process that allows a continuous control of measurements for the charging/discharging sequence. Data acquisition is fully automated and conducted in real time via suitable software. The applied voltage levels were: 10, 50, 100, 150, 200 and 240V. The applied temperatures were: 30, 60, 80, 100 and  $120^{\circ}\text{C}$ . Specimens were put between two electrodes in a parallel-plate capacitor configuration. The charging time was 60s for all the samples in every voltage level. Prior to every charging/discharging sequence, it was ensured that no stored charges exist in the samples with the implementation of a discharging short-circuit procedure. Measurements of the resistance in all samples were performed at 50, 100 and 200V. DC measurements were conducted according to the ASTM D257 specifications.

## 3. Results

### 3.1. Characterization of $\text{SrTiO}_3$ particles and $\text{SrTiO}_3$ nanocomposites

Bulk  $\text{SrTiO}_3$  undergoes a transition from the cubic paraelectric phase to the tetragonal antiferrodistortive phase at 104K, which is the  $T_c$  temperature [10]. Therefore, below the critical temperature nano  $\text{SrTiO}_3$  particles are in the cubic crystal phase. XRD patterns of  $\text{SrTiO}_3$  (Fig. 1a) indicate that nano  $\text{SrTiO}_3$  particles exist in cubic phase.

XRD spectrum indicates that the nano  $\text{SrTiO}_3$  particles are in cubic crystal phase (Pm3m). Although cubic phase is expected to be Raman inactive, because of the absence of polarizability, Fig. 1b shows that active Raman modes are detected in the cubic phase. Raman spectrum contains broad overlapping bands which are attributed to the second order Raman bands. Second order Raman bands derive from the creation of two phonons in the same vibrational branch resulting in overtone bands. Different overtone bands from different vibrations branches interfere resulting in the creation of one phonon and the destructions of another which has lower energy [11]. DSC thermograph (Fig. 1b inset) demonstrates that there is no phase transition in temperature range ( $-40^{\circ}\text{C}$  to  $200^{\circ}\text{C}$ ), leading to the deduction that the nano  $\text{SrTiO}_3$  phase transition occurs at lower temperatures as the theory implies ( $-169^{\circ}\text{C}$ ).

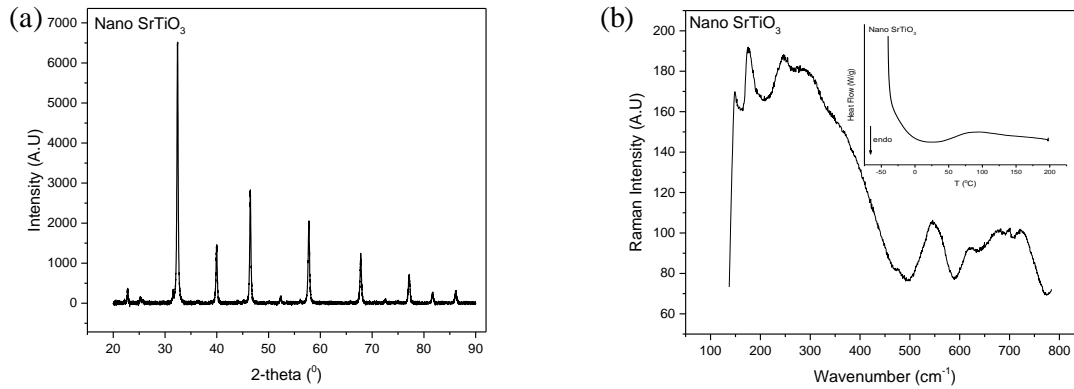


**Figure 1.** (a) XRD pattern of nano SrTiO<sub>3</sub> particles and (b) Raman spectrum of nano SrTiO<sub>3</sub> particles, inset shows its DSC thermograph.

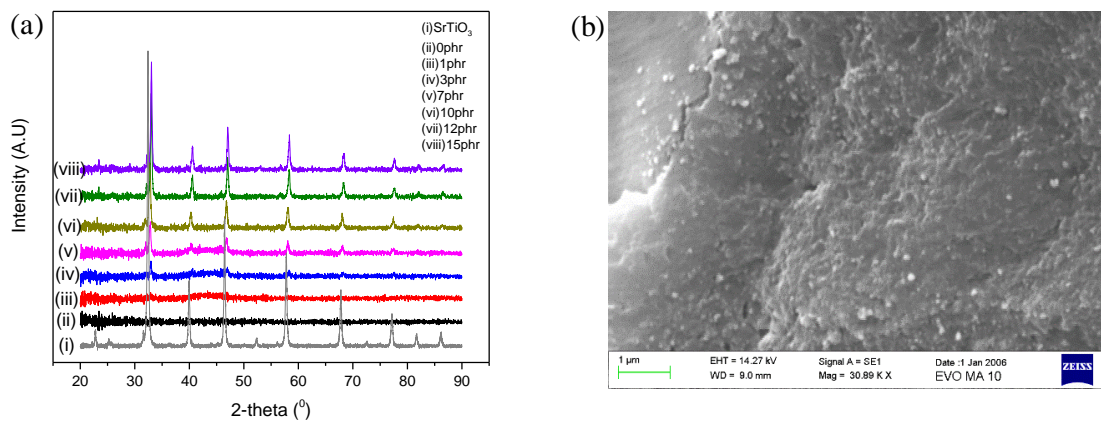


**Figure 2.** (a) XRD patterns of all fabricated nanocomposites and SrTiO<sub>3</sub> particles (b) SEM image for the 15phr SrTiO<sub>3</sub> nanocomposite.

Afterwards, the manufactured specimens were studied using X-ray diffraction method (XRD) and Scanning electron microscopy (SEM), in order to examine their morphology. XRD patterns are depicted in Fig. 2a. Epoxy resin as an amorphous component, has no diffraction peaks, as a result the deriving peaks in each nanocomposite systems correspond to the reinforced phase. It is apparent as the amount of the added nano-inclusions increases the peak owned to SrTiO<sub>3</sub> become sharper and more intense, indicating that there is a successful nanocomposite fabrication. Fig. 2b presents a SEM image for the 15phr SrTiO<sub>3</sub> nanocomposites. It is apparent that the dispersion of the nanofiller in the polymer matrix can be considered satisfactory, since fine nano-dispersions can be observed.

### 3.2 SrTiO<sub>3</sub> nanocomposite dielectric response

Dielectric spectra of composite systems are very complex, due to the interactions among molecules and/or particles and the concurrence of electric dipoles both permanent and induced. The SrTiO<sub>3</sub> nanocomposites systems were electrically characterized via BDS. 3D dielectric spectra of the real part of dielectric permittivity and loss tangent as a function of temperature and frequency, are represented for the 12phr SrTiO<sub>3</sub> nanocomposite in Figs. 3a and 3b respectively.

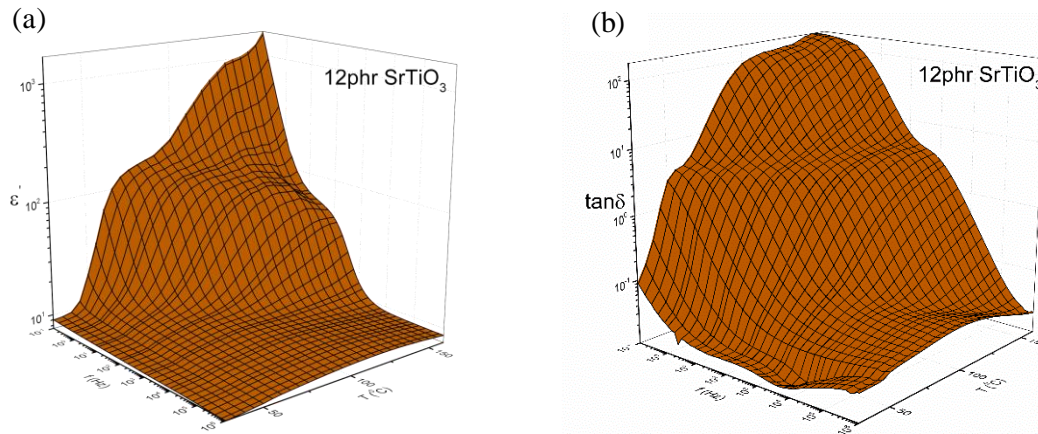


**Figure 3.** Dielectric spectra of the 12phr SrTiO<sub>3</sub> nanocomposite as a function of temperature and frequency, for the (a) real part of dielectric permittivity (left) and (b) loss tangent (right).

The nano SrTiO<sub>3</sub> reinforced systems exhibit higher values of  $\epsilon'$  in comparison with the neat epoxy in all frequency and temperature range.  $\epsilon'$  increases while the frequency of the applied field diminishes. This is because dipoles attain sufficient time to orient themselves in the direction of the alternating field. When frequency increases dipoles fail to follow the fast orientation of the applied field, resulting in low polarization level and  $\epsilon'$  values. The polarization process is facilitated by temperature, due to the thermal agitation of the dipoles and  $\epsilon'$  gets high values in the low frequency and high temperature range. Fig. 3a indicates a two step-like transition in the permittivity spectra, implying the presence of dielectric relaxation processes. The relaxation processes are more evident in the loss tangent versus temperature and frequency (Fig. 3b). At high frequencies and low temperatures, a weak relaxation process is observed which is assigned to the re-orientation of the polar side groups of the main polymer chain ( $\beta$ -relaxation). At intermediate frequencies and temperature, a stronger relaxation process is recorded. This transition is associated to the glass to rubber transition of the amorphous polymer matrix ( $\alpha$ -relaxation). The third relaxation occurs at low frequency and high temperature and is attributed to interfacial polarization (IP) process. Interfacial polarization process is observed in electrically heterogeneous systems of two or more phases. Since dipoles exhibit time delay in their orientation parallel to the field when the frequency of the applied field increases, as a result the appearance of the IP process is enhanced at low frequency edge and at high temperatures.

### 3.3 Energy storage and harvesting/ coefficient of energy efficiency

The storing and harvesting procedures for all specimens were studied by measuring the charging/discharging currents at various voltage levels and at different temperatures. The increase of the applied DC field leads to enhanced current in both charging and discharging processes. The discharging process takes place under no voltage field application. It has been revealed that all specimens exhibit similar behavior, and the DC applied field of 10V had experimental noise. It is well known that the stored energy is a function of capacitance, which is determined by the capacitor geometry and the permittivity of the material (Eq. 1) [13,14]. The stored energy is obtained by (Eq. 2)

$$C = \epsilon * \epsilon_0 * \frac{A}{d} \quad (1)$$

$$E = \int_0^Q V dq = \frac{1}{2} \frac{Q^2}{C} = \frac{1}{2} \frac{[\int I(t) dt]^2}{C} \quad (2)$$

where  $E$  is the energy of the capacitor,  $Q$  the accumulated charge,  $C$  the capacitance,  $\epsilon$  the dielectric constant,  $A$  the area of the capacitor's plate,  $d$  the distance of the capacitor's parallel plates, and  $\epsilon_0$  the dielectric constant of free space. In case of nanocomposite systems, the nanoinclusions act as a dispersive network of nanocapacitors. As Eq. 2 indicates the stored and harvested energy is determined via the time dependent charging and discharging currents at each temperature and applied voltage. The energies can be calculated by integrating the  $I=f(t)$  curves, in each case the specimen's capacitance is

determined by the dielectric measurements at the lowest measured frequency. Fig. 4 shows the stored and harvested energies of the 12phr SrTiO<sub>3</sub> nanocomposite, at 30°C and 80°C respectively

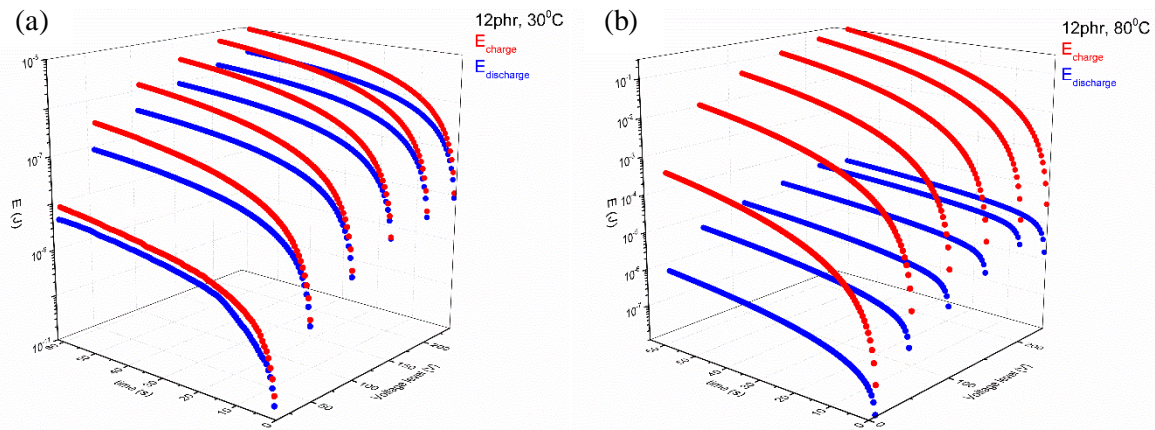


**Figure 4.** 3D spectra of stored and harvested energy as a function of time and DC voltage level for the 12phr SrTiO<sub>3</sub> nanocomposites at (a) 30°C (left) and at (b) 80°C (right).

Fig. 4 indicates that both stored and harvested energies elevate with the increase of the applied DC field. Furthermore, the energy efficiency seems to be decreased as the temperature increases. It would be very useful the introduction of a coefficient of energy efficiency in order to be able to evaluate the energy performance of the systems. The coefficient of energy efficiency is defined as the ratio of the retrieved upon stored energy (Eq. 3) [15].

$$n_{eff} = \frac{E_{discharged}}{E_{charged}} \quad (3)$$

The examined parameters are the temperature, the applied DC voltage, the time and the reinforcing phase. Fig. 5 shows that the  $n_{eff}$  decreases as the temperature increase. The same behaviour was observed in all specimens. For comparison reasons the stored and harvested energies are calculated at the time instant of 10s. Table 1 lists the  $n_{eff}$  values for all specimens at 30°C for three different applied voltage levels

Table 1 shows that the 10phr SrTiO<sub>3</sub> nanocomposite displays the optimum energy performance at 30°C reaching the value of  $n_{eff}=69.41\%$  at 50V. It is observed that the lowest applied DC field  $n_{eff}$  acquires the highest values in all nanocomposite systems except from the specimen with the higher filler content (15phr SrTiO<sub>3</sub>). The coefficient of energy efficiency is a quantity which can be affected by many parameters in different ways. Thus, the optimum performance does not always coincide with the highest filler content, because the nanofiller content is responsible for the heterogeneity of the systems and the formation of extended interface. The field intensity plays a major role in  $n_{eff}$ , considering that increases the number of charge carriers and facilitates the transportation of space charge within the nanocomposite by lowering the local potential barriers [16].

The influence of temperature upon  $n_{eff}$  for all nanocomposites at 50V is presented in Fig. 5. It is observed that only a sigmoid function could be used to fit the experimental results. Boltzmann sigmoid equation was applied via Eq. 4.

$$n_{eff} = \frac{A_1 - A_2}{1 + e^{(T - T_0)/dT}} + A_2 \quad (4)$$

where  $A_1$  is the initial value,  $A_2$  is the final value,  $T_0$  is the median.

**Table 1.** Coefficient of energy efficiency ( $n_{eff}$ %) for 50V, 100V and 200V at 30°C, for all SrTiO<sub>3</sub> nanocomposites

Applied voltage at 30°C for SrTiO <sub>3</sub> / nanocomposites	50V	100V	200V
1phr	44.61%	39.35%	44.34%
3phr	62.87%	53.38%	50.50%
7phr	37.31%	38.38%	38.80%
10phr	69.41%	42.01%	42.95%
12phr	46.26%	46.37%	47.80%
15phr	53.46%	44.51%	61.92%

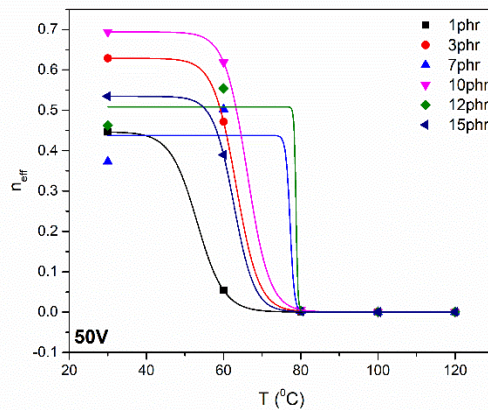


**Figure 5.** Boltzmann sigmoidal fitting for the coefficient of energy efficiency ( $n_{eff}$ ) at 50V as a function of temperature for all SrTiO<sub>3</sub> nanocomposites.

Fig. 5 indicates that the  $n_{eff}$  values at 60°C are high, and in some case, are higher than the respective ones at 30°C. Above 60°C, in all studied DC applied fields, temperature causes a dramatic decrease of  $n_{eff}$ . This  $n_{eff}$  decrease is associated with the significant augment of leakage currents. It can be argued that nano SrTiO<sub>3</sub> specimens display a different behavior from nano BaTiO<sub>3</sub> specimens [15]. Thus, the type of the filler plays major role in energy material performance. The fitting regressions show a quantitative estimation of the  $n_{eff} = f(T)$ . The same sigmoidal behavior of the  $n_{eff} = f(T)$  is observed in all three studied DC voltage levels. The fitting procedure had satisfactory regression so it can be concluded that the experimental data of  $n_{eff} = f(T)$  follow a sigmoidal function in all cases.

#### 4. Conclusions

Nanocomposite systems consisting of strontium titanate nanoparticles were fabricated and studied, varying the filler content of the reinforced phase. Both SrTiO<sub>3</sub> nanoparticles and nanocomposites were characterized by numerous techniques (XRD, LRS, DSC, SEM, BDS). In case of nanoparticles it was

verified that the nano SrTiO<sub>3</sub> particles were at paraelectric cubic phase. Nanocomposites were successfully fabricated (validation through XRD and SEM). Three relaxation processes have been detected in all examined dielectric spectra: (a) glass to rubber transition of the polymer matrix ( $\alpha$ -mode), (b) the rearrangement of the polar side groups of the main polymer chain ( $\beta$ -relaxation) and (c) IP effect. The ability of energy storage and harvesting was also investigated under DC conditions in all nanocomposite systems. Stored and harvested energies were determined by integrating the current-time function. It was found that both the stored and harvested energies increase with the applied DC voltage level. Coefficient of energy efficiency  $n_{eff}$  increases with the filler content reaching the values of 69.41% for the 10phr SrTiO<sub>3</sub> nanocomposite. The increase of temperature causes a sigmoidal behaviour of  $n_{eff}$  in all examined systems.

## References

- [1] C. Liu, F. Li, L-P. Ma and H-M. Cheng. Advanced Materials for Energy Storage. *Advanced Energy Materials*, 22: E28-E62, 2010.
- [2] J. Bae, M. K. Song, Y. J. Park, J. M. Kim, M. Liu and Z. L. Wang. Fiber Supercapacitors Made of Nanowire-Fiber Hybrid Structures for Wearable/Flexible Energy Storage. *Angewandte Chemie*, 50: 1683-1687, 2011.
- [3] M. S. Whittingham. Materials Challenges Facing Electrical Energy Storage. *Harvesting Materials for Energy*. 33: 411-419, 2008.
- [4] P. Khanchaitit, K. Han, M. R. Gadinski, Q. Li and Q. Wang. Ferroelectric polymer networks with high energy density and improved discharged efficiency for dielectric energy storage. *Nature Communication*. 4: 2845, 2013.
- [5] X. Zhao, B. M. Sanchez, P. J. Dobson and P. S. Grant. 2010. The Role of Nanomaterials in Redox-Based Supercapacitors for Next Generation Energy Storage Devices. *Nanoscale*, 3: 839-855, 2010.
- [6] G.C. Psarras. Nanodielectrics: an emerging sector of polymer nanocomposites. *Express Polymer Letters*, 2: 460, 2008.
- [7] I. Plesa, P.V. Notingher, S. Schlogl, C. Sumereder and M. Muhr. Properties of polymer composites used in high-voltage applications. *Polymers-Basel*, 8:173, 2016.
- [8] G.C. Psarras. Conductivity and dielectric characterization of polymer nanocomposites. Woodhead Publishing Limited, 2010.
- [9] H. B. Radousky and H. Liang. Energy Harvesting: An Integrated View of Materials, Devices and Applications. *Nanotechnology*, 23:502001, 2012.
- [10] Y-P. Cai, D. -Z. Han and R-Y. Ning. Theoretical Study of Antiferrodistortive Phase Transition in Strontium Titanate. *Chinese Journal of Chemical Physics*, 23:237-240, 2010.
- [11] W. G. Nilsen, J. G. Skinner. Raman Spectrum of Strontium Titanate. *Journal of Chemical Physics*, 4:2240-2248, 1968.
- [12] Y.I. Yuzyuk. Raman scattering spectra of ceramics, films, and superlattices of ferroelectric perovskites: A review. *Physics of the Solid State*, 54:1026-1059, 2012.
- [13] X. Hao. A review on the dielectric materials for high energy-storage application, *Journal of Advanced Dielectrics*, 3: 1330001, 2013.
- [14] Y. Imanaka, H. Amada and F. Kumasaka. Microstructure and dielectric properties of composite films for embedded capacitor applications. *International Journal of Applied of Ceramic Technology*, 8:653-657, (2011).
- [15] G.C. Manika and G.C. Psarras. Energy storage and harvesting in BaTiO<sub>3</sub>/epoxy nanodielectrics. *High Voltage*, 1:151-157, 2016.
- [16] J.R. Dennison and J. Brunson. Temperature and electric field dependence of conduction in low-density polyethylene *IEEE Transactions on Plasma Science*, 36: 2246-2252, 2008.